CHARACTERIZATION AND OPTICAL STUDIES OF HYBRID MATERIALS SYNTHESIZED BY COVALENTLY LINKING Eu^{3+} IONS, PARA-AMINOBENZOIC ACID, AND TITANIA[**]

T. Jesty [*], K. S. Ambili, A. M. Baby, S. Sonyamol

Kuriakose Elias College, Mannanam, Kottayam, Kerala, 686561, India; e-mail: jestyk@gmail.com

Two new luminescent hybrid materials were synthesized using para-aminobenzoic acid (PABA), europium nitrate, and titania. Characterization of the synthesized hybrid materials using infrared spectroscopy and CHN elemental analysis revealed the bonding sites and compositions of the two hybrid materials. The homogenous nature of the hybrid materials was confirmed by scanning electron microscopy. The optical properties of these synthesized materials were studied using UV-visible absorption spectroscopy and photoluminescence spectroscopy. Thermogravimetric analysis revealed that the hybrid materials are thermally stable.

Keywords: *inorganic-organic hybrid material, photoluminescence, titania.*

ХАРАКТЕРИСТИКА И ОПТИЧЕСКИЕ ИССЛЕДОВАНИЯ ГИБРИДНЫХ МАТЕРИАЛОВ, СИНТЕЗИРОВАННЫХ КОВАЛЕНТНЫМ СВЯЗЫВАНИЕМ ИОНОВ Eu^{3+}, ПАРААМИНОБЕНЗОЙНОЙ КИСЛОТЫ И ИЗОПРОПОКСИДА ТИТАНА

T. Jesty [*], K. S. Ambili, A. M. Baby, S. Sonyamol

УДК 535.37:546.821/.824

Колледж Куриакос Элиас, Маннанэм, Коттаям, Керала, 686561, Индия; e-mail: jestyk@gmail.com

(Поступила 1 марта 2016)

С использованием парааминобензойной кислоты, нитрата европия и изопропилата титана синтезированы два новых люминесцирующих гибридных вещества. Исследование их характеристик с использованием ИК спектроскопии и элементного CHN-анализа выявило места связывания и состав гибридных материалов. Однородность структуры гибридных материалов подтверждена методом сканирующей электронной микроскопии. Оптические свойства синтезированных материалов исследованы с помощью абсорбционной спектроскопии в УФ и видимой областях спектра и фотолюминесцентной спектроскопии. Термогравиметрический анализ показал, что полученные гибридные материалы термически стабильны.

Ключевые слова: *органическо-неорганический гибридный материал, фотолюминесценция, диоксид титана.*

Introduction. There has been increasing interest in the design, synthesis, and development of lanthanides containing organic complexes due to their exceptional luminescence properties. The luminescence properties of lanthanide organic complexes result from the intramolecular energy transfer ("antenna effect") between the ligand and chelated metal ion [1]. These complexes find applications in different fields like organic light emitting diodes (OLEDs), sensors, molecular optoelectronic devices, etc. But their poor mechanical and thermal stability limits their exploration in many fields [2, 3]. Recently, there has been an increased attention to the development of lanthanide containing inorganic-organic hybrid materials as they can combine the advantages of an inorganic part like high thermal and mechanical stability and also the benefits of an organic part like synthetic versatility, luminescence property, etc. Thus inorganic-organic hybrid materi-

[**] Full text is published in JAS V. 84, No. 1 (http://springer.com/10812) and in electronic version of ZhPS V. 84, No. 1 (http://www.elibrary.ru/title_about.asp?id=7318; sales@elibrary.ru).

als synthesized by fabricating organic complexes into inorganic matrices shows integrated properties of organic and inorganic parts simultaneously [4].

There are mainly two types of inorganic-organic hybrid materials. In the type of hybrid materials which are formed by the physical mixing of the two components, the interaction between organic and inorganic parts is caused by weak van der Waals forces. The inhomogeneous distribution and clustering of lanthanide ions in this type of hybrids results in a decrease in luminescence intensity. On the other hand, in hybrid materials of the second type, the chemical interaction is due to the covalent bonds between the inorganic and organic components. These materials show homogenous distribution, enhanced luminescence properties, and thermal stability. The luminescence properties and stability of silica based lanthanide containing hybrid materials linked by chemical interaction are widely studied because of their built-in robustness and tunable physical properties [5–8]. The synthesis and properties of hybrid materials containing other inorganic matrices like zirconia, titania, and alumina are rarely reported [9]. In the present work we have synthesized two titania based hybrid materials PABA-Ti-Eu and PABA-Eu-Ti where the interaction between the inorganic and organic parts is through strong covalent bonds. The luminescence properties and thermal stability of the two materials were compared.

Experimental. Para-aminobenzoic acid (PABA) and ethanol were purchased from M/S Merk Chemicals. Europium(III) nitrate and titanium(IV) isopropoxide were purchased from Sigma Aldrich. All the chemicals were used without further purification. Distilled water was used throughout the experiment.

Synthesis of hybrid material (PABA-Ti-Eu). A 1.136 g portion of titanium isopropoxide was added to 20.0 ml of 4.0 mmol solution of PABA in absolute ethanol. The mixture was then refluxed for 30 min to form a yellow colored solid powder (PABA-Ti). A 0.213 g portion of $Eu(NO_3)_3$ dissolved in absolute ethanol was added to this and refluxed for 1 h. The bright orange colored powder formed was collected, washed with ethanol, and dried. The product is designated as S_1.

Synthesis of hybrid material (PABA-Eu-Ti). Another material was also synthesized using the same precursors and the same procedure but by changing the sequence of addition of precursors. A 0.213 g portion of $Eu(NO_3)_3$ was added to 20.0 ml of 4.0 mmol solution of PABA in absolute ethanol with stirring. The mixture was then refluxed for 30 min to form white colored PABA-Eu complex. A 1.136 g portion of titanium isopropoxide was added to this and refluxed for 1 h. The yellow colored powder formed was collected, washed with ethanol, and dried. The product is designated as S_2.

Elemental analyses were carried out on an Elementar Vario EL III instrument. FTIR spectra were taken within 400–4000 cm^{-1} region on a Perkin-Elmer Spectrum 400FTIR/FTFIR spectrophotometer. The powder X-ray diffraction patterns were obtained on a Bruker D8 advanced diffractometer. Scanning electron microscopic (SEM) images were obtained from a JEOM JSM-6700 field-emission scanning electron microscope. UV-visible absorption spectra were recorded on a UV-2400PC series spectrophotometer, and fluorescence excitation and emission spectra were obtained on a SL174 spectrofluorometer using 150 W Xenon lamp as excitation source. A Shimadzu DTG-60 instrument was used for recording the thermogram of the synthesized materials.

Results and discussion. The molecular formulas of S_1 and S_2 were obtained from the CHN elemental analysis. S_1 has the molecular formula $C_{28}H_{24}EuN_6O_{22}Ti_8$ (1331.4) (Calculated: C 25.1, H 2.8 N 6.28, Found: C 26.9, H 2.3, N 6.5). The predicted structure for the hybrid material S_1 is shown in Fig. 1a. The molecular formula of S_2 is obtained as $C_{66}H_{73}Eu_5N_8O_{21}Ti_2$ (2168) (Calculated: C 36.5, H 3.36, N 5.16, Found: C 36, H 3.37, N 5.18). The predicted structure for S_2 is shown in Fig.1b.

Details of the IR spectra of PABA (ligand), PABA-Ti network, PABA-Eu complex, S_1, and S_2 are shown in Table 1. The difference between asymmetric and symmetric stretching vibration of carboxylate group of PABA was found to be 184 cm^{-1} ($\nu_{as} - \nu_s = 1599 - 1415$ cm^{-1}). It is decreased to 164 cm^{-1}($\nu_{as} - \nu_s =$ $= 1551 - 1387$ cm^{-1}) in the PABA-Ti network, which indicates that the bond formation to Ti in PABA-Ti is through the carboxylate group of PABA. The peak at 3462 cm^{-1} of free PABA is due to the N–H stretching vibration of the amino group. The peak is shifted to 3435 cm^{-1} in S_1, indicating bond formation through the amino group of PABA to Eu^{3+} in S_1.

The difference between asymmetric and symmetric stretching vibration of carboxylate group of PABA was found to increase to 201 cm^{-1} ($\nu_{as} - \nu_s = 1599 - 1398$ cm^{-1}) in PABA-Eu complex. This indicates that the bond formation is through the carboxylate group of PABA to Eu^{3+} in PABA-Eu [10]. Absence of N–H stretching vibration of PABA in S_2 indicates that the bond formation is through the amino group of PABA to Ti in S_2 [11]. Other characteristic peaks at 1173 and 1131cm^{-1} due to C–H stretching vibration and peak at 1310 cm^{-1} due to C–N stretching vibration of amino group of PABA were observed in all samples [12].

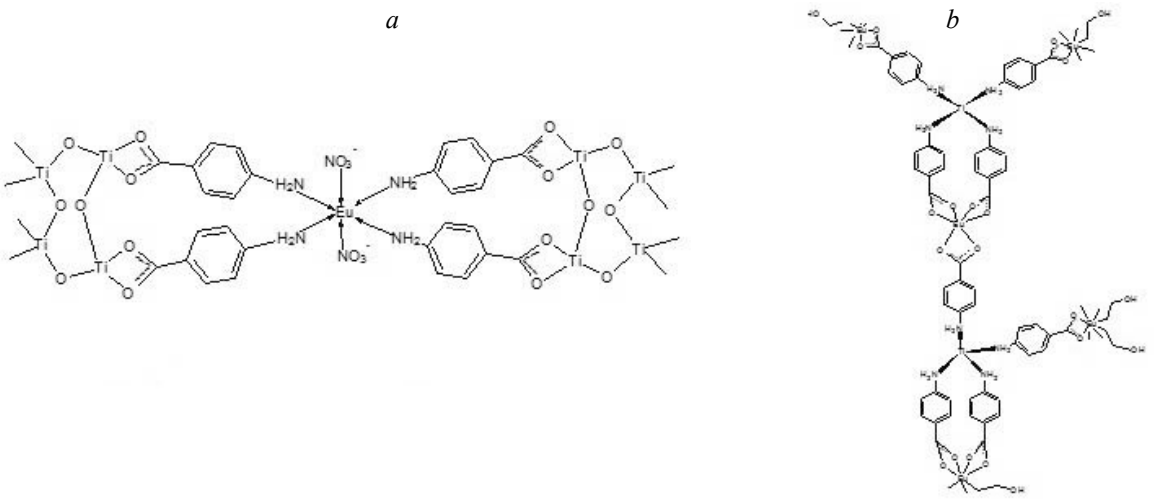

Fig. 1. Proposed structure of S_1 (a) and S_2 (b).

TABLE 1. Assignments of Infrared Absorption Bands (cm^{-1}) of PABA, PABA-Ti, S_1, PABA-Eu, and S_2

Characteristic	PABA	PABA-Ti	S_1	PABA-Eu	S_2
$\Delta (\nu_{as} - \nu_s) COO^-$	184 (1599–1415)	164 (1551–1387)	164 (1551–1387)	201 (1599–1398)	201 (1599–1398)
N–H stretching	3462	3462	3435	3462	–
C–H stretching	1173, 1131	1173, 1131	1173, 1131	1173, 1131	1173, 1131
C–N stretching	1310	1310	1310	1310	1310

The PXRD patterns of S_1 and S_2 (Fig. 2) shows Bragg peaks at low reflection angles which is typical of porous materials [13]. Other Bragg peaks of sample S_2 become weak and diffuse, implying poor crystallinity. The XRD patterns of S_1 and S_2 are dissimilar, indicating that the atomic distribution is different in the two samples. Product S_1 shows strong and sharp peaks compared to S_2 which can be attributed to its crystalline nature as a result of the regular arrangement of Ti–O network in S_1. But in S_2 the distribution of organic groups is less ordered, which results in diffused peaks in its XRD pattern [14].

Figure 3 shows the SEM images of S_1 and S_2. Both the hybrid materials showed uniform distribution, and there is no separation between the organic and inorganic phases. The hybrid material S_1 shows more regular and uniform microstructure than S_2 [15]. This may be due to the difference in the network structure formed in S_1 and S_2. In S_1 the organic and inorganic phases are linked through the carboxylate group of PABA and form a Ti–O network system that is more stable and regularly arranged, whereas in S_2, Ti^{4+} is coordinated to the ligand through NH_2 and forms a different network structure that is less orderly distributed [16].

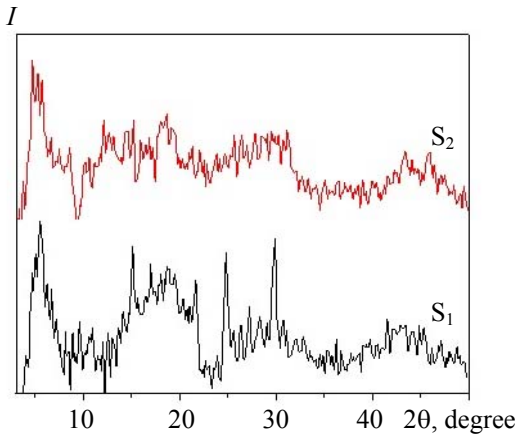

Fig. 2. PXRD patterns of S_1 and S_2.

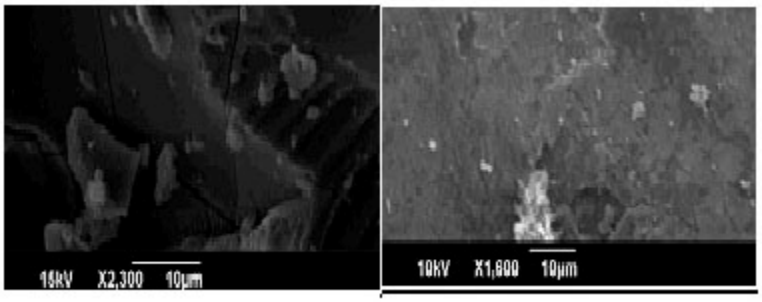

Fig. 3. SEM images of S_1 and S_2.

Figure 4 shows the solid state absorption spectra of PABA, S_1 and S_2. The absorption spectra show two main peaks at 260 and 337 nm for the PABA ligand. The hybrid materials also show absorption in this region due to absorption of the PABA part. PABA shows significant absorption only up to 400 nm, and the complex shows more absorption than the ligand due to the formation of the extensive coordination environment of the complex [17]. Also the region of absorption is further enhanced in S_1 because of the presence of the Ti–O network structure [18, 19].

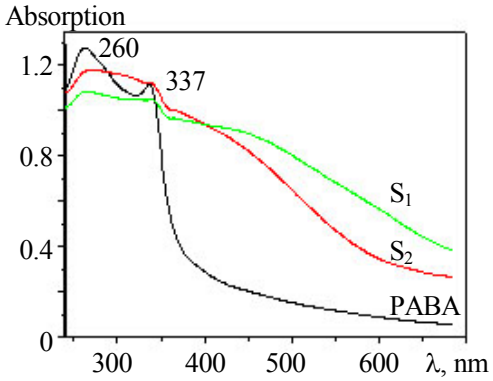

Fig. 4. UV-Visible absorption spectra of PABA, S_1 and S_2.

Figure 5 shows the thermogravimetric traces and differential thermogravimetric traces of S_1 and S_2. The thermal degradation of S_1 occurs in three main stages. During the first stage, from 39.1 to 131°C, a weight loss of 7.2% is observed due to the removal of solvent. The second stage shows a weight loss of 15.61% from 131 to 321°C due to the removal of physically adsorbed water molecule and the decomposition of organic ingredients formed due to the polycondensation reaction of titanium isopropoxide [20]. The degradation of the organic part, which takes place between 321 and 624°C, results in a weight loss of 18.06 %.

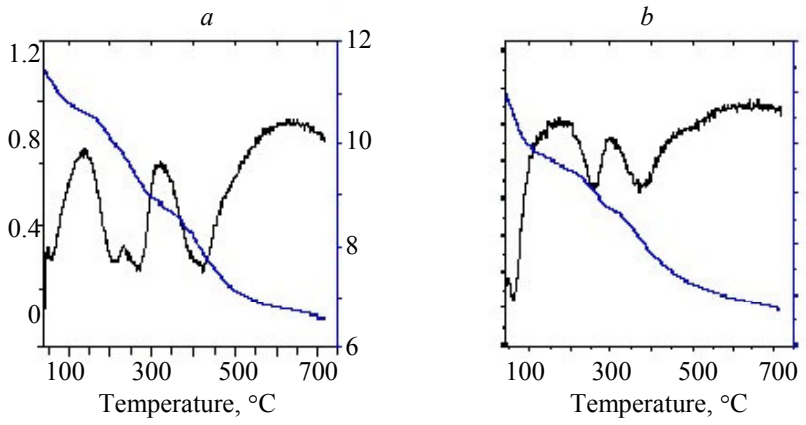

Fig. 5. TG-DTG spectra of S_1 (a) and S_2 (b).

The thermal degradation of S_2 also occurs in three main stages. During the first stage from 37.17 to 121°C, a weight loss of 11.9% is observed due to the removal of solvent ethanol. The second stage shows a weight loss of 9.4% from 121 to 299°C due to the removal of physically adsorbed water molecule. The degradation of the organic part starts from 299°C and shows a 17.2% weight loss. The results demonstrate that the sample S_1 shows better thermal stability than the sample S_2 because of the Ti–O-network structure.

It is reported that PABA ligand can influence the sensitization of Eu^{3+} luminescence [21]. But the functionalization of PABA by the network structure in S_1 and S_2 quenches the excitation energy of PABA due to coordination. Both S_1 and S_2 have an intensive emission at a wavelength 612 nm under the direct excitation of Eu^{3+} at 413, 446, and 476 nm (Fig. 6). The quenching effect due to the functionalization of PABA and the network decreases the energy transfer from ligand to Eu^{3+} and hence decreases the luminescence of Eu^{3+}. From the excitation spectrum it is clear that the intensity of the S_1 direct excitation peaks is less compared to S_2, which shows that the indirect excitation is more favorable in S_1. Also the quenching effect for the excitation peaks of PABA in sample S_1 is less compared to S_2 and hence S_1 can give better luminescence properties than S_2, which is in a good agreement with the earlier report [20]. The emission spectra of S_1 and S_2 at an excitation wavelength 413 nm showed characteristic emission peaks of Eu^{3+}. The emission peak at 551 nm is due to the $^5D_1$ to $^7F_1$ transition, and the peaks at 612 and 651 nm are due to the $^5D_0 \rightarrow {}^7F_2$ and $^5D_0 \rightarrow {}^7F_3$ transitions, respectively [22].

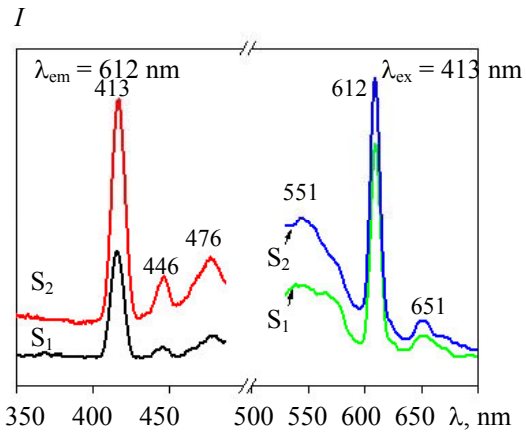

Fig. 6. Solid state excitation spectra (λ_{em} = 612 nm) and emission spectra (λ_{ex} = 413 nm) of S_1 and S_2.

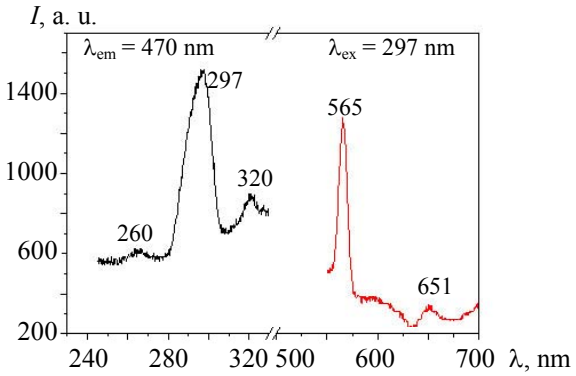

Fig. 7. Solid state excitation spectrum (λ_{em} = 470 nm) and emission spectrum (λ_{ex} = 297 nm) of S_1.

On comparing the luminescence of S_1 and S_2, the solid state room temperature excitation spectra of S_1 at an emission wavelength 470 nm (Fig. 7) showed excitation peaks at 260, 297, and 320 nm due to the excitation of PABA modified Ti–O network, whereas these peaks are not observed for S_2 at this emission wavelength. This excitation spectrum of S_1 overlaps with the absorption spectrum of the ligand. It indicates that

the intramolecular energy transfer from ligand to metal occurs in S_1. The absence of these excitation peaks at this emission wavelength in S_2 reveals that the ligand to metal energy transfer is quenched in S_2. The emission spectrum of S_1 at an excitation wavelength 297 nm also shows characteristic emission peaks of Eu^{3+}. Here the higher intensity peak is at 565 nm due to $^5D_1 \rightarrow {}^7F_1$ transition. Peak at 651 nm due to $^5D_0 \rightarrow {}^7F_3$ is also obtained in the emission spectrum. Hence S_1 shows better luminescence properties than S_2, and the difference in luminescence is due to the different network structures resulting from different coordination sites in the two samples.

Conclusion. Two titania based hybrid luminescent and thermostable materials were synthesized using PABA and europium. IR spectroscopy and CHN elemental analysis were used to investigate coordination sites of the organic and inorganic parts of the hybrid materials. The sequence of addition of precursors during synthesis of these materials changed the coordination sites of organic and inorganic parts of the hybrid materials. The material PABA-Ti-Eu (S_1) showed better stability, luminescence, and more homogenous structure than PABA-Eu-Ti (S_2) because of the difference in coordination between inorganic and organic parts in the two materials. The results indicate that the synthesized hybrid material, PABA-Ti-Eu (S_1), can be used as a promising, stable candidate for luminescent applications.

Acknowledgment. This work is financially supported by the Department of Science and Technology (DST), New Delhi, India under “Fast Track Young Scientist Scheme” (No: SR/FT/CS-33/2011).

REFERENCES

1. L. Zhai, W.-W. Zhang, X.-M. Ren, J.-L. Zuo, *Dalton Trans.*, **44**, 5746–5754 (2015).
2. Y. Chen, R. Guan, C. Zhang, J. Huang, L. Ji, H. Chao, *Coord. Chem. Rev*., **310**, 16–40 (2016).
3. P. C. S. Filho, J. F. Lima, O. A. Serra. *J. Braz. Chem. Soc*., **26**, 2471–2495 (2015).
4. X. Guo, J.-L. Canet, D. Boyer, P. Adumeau, R. Mahiou, *J. Sol-Gel Sci. Technol.*, **64**, 404–410 (2012).
5. H. Lu, H. Wang, and S. Feng, *J. Photochem. Photobiol., A*, **210**, 48–53 (2010).
6. L. Guo, L. Fu, R. A. S. Ferreira, L. D. Carlos, B. Yan, *J. Solid State Chem*., **194**, 9–14 (2012).
7. L. Guo, B. Yan, *Inorg. Chem. Commun.*, **14**, 1833–1837 (2011).
8. Y.-J. Gu, B. Yan, X.-F. Qiao, *J. Solid State Chem.*, **199**, 116–122 (2013).
9. L. Guo, B. Yan, *J. Photochem. Photobiol., A*, **224**, 141–146 (2011).
10. Y. Li, F.-P. Liang, *Inorg. Chim. Acta*, **361**, 219–225 (2008).
11. A. Burak, Y. Emel, *Inorg. Chim. Acta*, **399**, 208–213 (2013).
12. N.V Roik, N. A. Belyakova, *Phys. Chem. Solid State*, **12**, 168–173 (2011).
13. S. Zheng, L. Gao, J. Guo, *Mater. Chem. Phys*., **71**, 174–178 (2001).
14. B.Yan, H.-F. Lu, *J. Photochem. Photobiol., A*, **205**, 122–128 (2009).
15. X. Qiao, B. Yan, *J. Organomet. Chem*., **694**, 3232–3241(2009).
16. K. sheng, B. Yan, X.-F. Qiao, *J. Fluoresc*., **21**, 653–662 (2011).
17. F. Yali, Z. Jingchang, L. Yuguang, C. Weiliang, *Spectrochim. Acta, A*, **70**, 646–650 (2008).
18. Y.-Y. Ren, B.-L. An, X. Qian, *J. Alloys Compd*., **501**, 42–46 (2010).
19. K. Sheng, B. Yan, *J. Photochem. Photobiol.*, *A*, **206**, 140–147(2009).
20. X.-L. Wang, B. Yan, *Colloid. Polym. Sci.*, **289**, 423–431 (2011).
21. S. Wu, Y. Chen, Z. Xing, S. Cao, X. Geng, Y. Xie, Y. Li, *Acta Opt. Sin.*, **1**, 313–320 (2015).
22. R. Shyni, M. L. P. Reddy, K. V. Vasudevan, A. H. Cowley, *Dalton Trans*., **41**, 14671–14682 (2012).